BIT Numerical Mathematics (2021) 61:1397–1419
https://doi.org/10.1007/s10543-021-00865-0

BIT

An exponential integrator sine pseudospectral method for the generalized improved Boussinesq equation

Chunmei Su[1,2] · **Gulcin M. Muslu**[3]

Received: 27 May 2020 / Accepted: 26 March 2021 / Published online: 23 April 2021

Abstract
A Deuflhard-type exponential integrator sine pseudospectral (DEI-SP) method is proposed and analyzed for solving the generalized improved Boussinesq (GIBq) equation. The numerical scheme is based on a second-order exponential integrator for time integration and a sine pseudospectral discretization in space. Rigorous analysis and abundant experiments show that the method converges quadratically and spectrally in time and space, respectively. Finally the DEI-SP method is applied to investigate the complicated and interesting long-time dynamics of the GIBq equation.

Keywords Error estimate · Exponential integrator · Improved Boussinesq equation · Long-time dynamics · Sine pseudospectral method

Mathematics Subject Classification 35Q53 · 65M15 · 65M70

1 Introduction

The Boussinesq equation was originally proposed by Boussinesq in 1870s to describe the nonlinear wave propagations in multiple directions [5,6]. Similar to the Korteweg-de Vries (KdV) equation, which was derived in 1895 to describe the wave moving in the positive direction [18], the Boussinesq equation describes a wide class of nonlinear dispersive wave phenomena and is applied in many fields. For instance, the Boussinesq

Communicated by Christian Lubich.

✉ Gulcin M. Muslu
gulcin@itu.edu.tr

Chunmei Su
sucm13@163.com

1 Yau Mathematical Sciences Center, Tsinghua University, Beijing 100084, China

2 Zentrum Mathematik, Technische Universität München, 85748 Garching bei München, Germany

3 Department of Mathematics, Istanbul Technical University, 34469 Maslak, Istanbul, Turkey

equation models the simulation of water waves in shallow seas and harbors in coastal engineering, and propagation of ion-sound waves in a uniform isotropic plasma [20]. Generally, the Boussinesq equation has the form

$$z_{tt} = z_{xx} + q z_{xxxx} + (z^2)_{xx}, \tag{1.1}$$

which for $q = 1$ gives the bad or ill-posed Boussinesq (BBq) equation [8], while for $q = -1$ the good or well-posed Boussinesq (GBq) equation [21]. For the well-posed GBq equation, there have been extensive literature on the well-posedness and numerical studies (see [15,17,21,23,24] and references therein). As was shown in [3], the BBq equation is unstable under short wave perturbation and there is no local well-posedness result. However, the BBq equation could be approached by the improved Boussinesq (IBq) equation by replacing the term z_{xxxx} with z_{xxtt},

$$z_{tt} = z_{xx} + z_{xxtt} + (z^2)_{xx}, \tag{1.2}$$

which is physically stable and well suited for mathematical modelling work [3,20]. In fact, the IBq equation is applied to describe the propagation of acoustic waves on elastic rods [26] and the propagation of plasma waves at right angles to the magnetic field [2]. Furthermore, the IBq equation satisfies some conservation laws, e.g., *mass* and *energy* [30]:

$$\mathscr{M} = \int_{\mathbb{R}} z \, dx, \quad \mathscr{H} = \int_{\mathbb{R}} \left(v^2 + z^2 + \frac{2}{3} z^3 + (z_t)^2\right) dx, \tag{1.3}$$

where $z_t = v_x$.

The IBq equation has been investigated theoretically and numerically in recent years. Yang [31] studied the local, global well-posedness and non-existence of global solutions to the initial and boundary value problem for the IBq equation. The existence of the global classical solutions and the blow-up of the solution for the initial and boundary value problem were also studied in [11]. Furthermore, the authors in [32] investigated the existence and uniqueness of the generalized solution of IBq equation for the initial and boundary value problem using a Galerkin approximation scheme combined with the continuation of solutions step by step and the Fourier transform method. They also proved that the solution blows up in finite time under appropriate conditions on initial data. Recently, the controllability of the IBq equation posed on a bounded or periodic domain was considered in [9]. For the numerical part, there have been a large amount of works in the literature for the IBq equation, ranging from finite difference methods [7,8], finite element methods [16,19], spectral method [4], meshless method [25], Runge-Kutta type exponential integrators [22] and energy-preserving methods [28,30]. Different methods were applied to investigate abundant dynamics of the IBq equation, however, there are quite few works on the rigorous error estimates for the corresponding numerical methods. Most of the time, the authors only gave some stability analysis or conservation properties. The convergence of the semi-discrete scheme for a Fourier pseudospectral method was proved in [4].

In this work, we consider the IBq equation with general nonlinearity (GIBq):

$$\begin{cases} z_{tt} = z_{xx} + z_{xxtt} + (f(z))_{xx}, \\ z(x,0) = z_0(x), \quad z_t(x,0) = z_1(x), \end{cases} \tag{1.4}$$

where $f \in C^\infty(\mathbb{R},\mathbb{R})$. The cubic nonlinearity was proposed and the corresponding dynamics was investigated in [12] to study the acoustic waves on elastic rods, where the equation for cubic nonlinearity was called the modified improved Bousssinesq equation. We'll apply a second-order exponential integrator sine pseudospectral method to solve (1.4) and give an unconditional convergence in a general energy norm.

The rest of this paper is organized as follows. In Sect. 2, we propose a Deuflhard-type exponential integrator sine pseudospectral method for the GIBq equation. The main error estimate is carried out in Sect. 3. Section 4 is devoted to presenting some numerical results to illustrate the convergence result and to show rich dynamics of the GIBq equation. Finally, some concluding remarks are drawn in Sect. 5. Throughout this paper, C denotes a generic constant independent of the mesh size and the time step, and $C(p,q)$ means C depends on p and q.

2 Exponential integrator sine pseudospectral method

In this section, we present the exponential integrator sine pseudospectral method for the GIBq equation, based on a Deuflhard-type exponential integrator combined with a sine pseudospectral discretization in space. For practical implementation, we truncate the GIBq equation on a bounded domain $\Omega = (a,b)$ with homogeneous boundary conditions (here $|a|$ and b are chosen large enough such that the truncation error is negligible):

$$\begin{cases} z_{tt}(x,t) = z_{xx}(x,t) + z_{xxtt}(x,t) + (f(z))_{xx}(x,t), \quad x \in \Omega, \quad t > 0, \\ z(x,0) = z_0(x), \quad z_t(x,0) = z_1(x), \\ z(a,t) = z(b,t) = 0, \quad z_{xx}(a,t) = z_{xx}(b,t) = 0, \quad t \geq 0, \end{cases} \tag{2.1}$$

where $f \in C^\infty(\mathbb{R},\mathbb{R})$.

For the full discretization of (2.1), we introduce some discrete spaces firstly. The interval $[a,b]$ is divided into M equal subintervals with grid spacing $h = (b-a)/M$, with M a positive integer. The spatial grid points are given by $x_j = a + jh$, $j = 0, 1, 2, \ldots, M$. The time interval $[0,T]$ is divided into N equal subintervals with time step $\tau = T/N$ and temporal grid points $t_n = n\tau$, $n = 0, \ldots, N$. Denote

$$\begin{aligned} X_M &:= \{u = (u_0, u_1, \ldots, u_M) \in \mathbb{R}^{M+1} | u_0 = u_M = 0\}, \\ Y_M &:= \text{span}\{\sin(\mu_l(x-a)), \quad l = 1, 2, \ldots, M-1\}, \end{aligned}$$

with $\mu_l = \frac{l\pi}{b-a}$. For a general function $u(x)$ on $\overline{\Omega} = [a,b]$ and a vector $u \in X_M$, let $P_M : L^2(\Omega) \to Y_M$ be the standard L^2-projection operator and $I_M : C_0(\overline{\Omega}) \to Y_M$ or $I_M : X_M \to Y_M$ be the trigonometric interpolation operator as

$$(P_M u)(x) = \sum_{l=1}^{M-1} \widehat{u}_l \sin(\mu_l(x-a)), \quad (I_M u)(x) = \sum_{l=1}^{M-1} \widetilde{u}_l \sin(\mu_l(x-a)), \tag{2.2}$$

where $\widehat{u}_l$ and $\widetilde{u}_l$ are the sine and discrete sine transform coefficients, respectively, defined as

$$\widehat{u}_l = \frac{2}{b-a}\int_a^b u(x)\sin(\mu_l(x-a))dx, \qquad \widetilde{u}_l = \frac{2}{M}\sum_{j=1}^{M-1} u_j \sin\left(\frac{jl\pi}{M}\right), \tag{2.3}$$

with $u_j = u(x_j)$ when involved.

The sine pseudospectral discretization is to find $z_M(x,t) \in Y_M$, i.e.,

$$z_M(x,t) = \sum_{l=1}^{M-1} \widehat{z}_l(t)\sin(\mu_l(x-a)), \tag{2.4}$$

such that

$$\partial_{tt} z_M = \partial_{xx} z_M + \partial_{xxtt} z_M + \partial_{xx} P_M(f(z_M)). \tag{2.5}$$

Substituting (2.4) into (2.5) and noticing the orthogonality of $\sin(\mu_l(x-a))$, we have for $t_n = n\tau$ and $s \in \mathbb{R}$,

$$(1+\mu_l^2)\frac{d^2}{ds^2}\widehat{z}_l(t_n+s) + \mu_l^2 \widehat{z}_l(t_n+s) + \mu_l^2 \widehat{(f_M^n)}_l(s) = 0, \tag{2.6}$$

where $f_M^n(x,s) = f(z_M(x,t_n+s))$. By using the variation of constants formula, we get

$$\widehat{z}_l(t_n+s) = \cos(\theta_l s)\widehat{z}_l(t_n) + \frac{\sin(\theta_l s)}{\theta_l}\widehat{z}_l{}'(t_n) - \theta_l \int_0^s \widehat{(f_M^n)}_l(w)\sin(\theta_l(s-w))dw, \tag{2.7}$$

where $\theta_l = \mu_l/\sqrt{1+\mu_l^2}$. Differentiating (2.7) with respect to s, we obtain

$$\widehat{z}_l{}'(t_n+s) = -\theta_l \sin(\theta_l s)\widehat{z}_l(t_n) + \cos(\theta_l s)\widehat{z}_l{}'(t_n) - \theta_l^2 \int_0^s \widehat{(f_M^n)}_l(w)\cos(\theta_l(s-w))dw. \tag{2.8}$$

Substituting $s = \tau$ in (2.7) and (2.8), followed by applying the standard trapezoidal rule or the Deuflhard-type quadrature [13] for approximating the integrations, we get

$$\begin{aligned}
\widehat{z_l}(t_{n+1}) &\approx \cos(\theta_l\tau)\widehat{z_l}(t_n) + \frac{\sin(\theta_l\tau)}{\theta_l}\widehat{z_l}'(t_n) - \frac{\theta_l\tau}{2}\sin(\theta_l\tau)\widehat{(f_M^n)}_l(0),\\
\widehat{z_l}'(t_{n+1}) &\approx -\theta_l\sin(\theta_l\tau)\widehat{z_l}(t_n) + \cos(\theta_l\tau)\widehat{z_l}'(t_n)\\
&\quad - \frac{\theta_l^2\tau}{2}\left[\cos(\theta_l\tau)\widehat{(f_M^n)}_l(0) + \widehat{(f_M^n)}_l(\tau)\right].
\end{aligned} \tag{2.9}$$

In practice, computing the continuous sine coefficients is difficult from the integration formula given in (2.9). Therefore, we replace the continuous sine coefficients by the discrete sine coefficients as in (2.3). A detailed Deuflhard-type exponential integrator sine pseudospectral (DEI-SP) method reads as follows. Denote z_j^n and $\dot{z}_j^n (j = 0, 1, \ldots, M, n = 0, 1, \ldots)$ by the approximations to $z(x_j, t_n)$ and $\partial_t z(x_j, t_n)$, respectively. Setting $z_j^0 = z_0(x_j)$, $\dot{z}_j^0 = z_1(x_j)$, then for $n \geq 0$,

$$z_j^{n+1} = \sum_{l=1}^{M-1} \widetilde{z_l^{n+1}} \sin\left(\frac{jl\pi}{M}\right), \quad \dot{z}_j^{n+1} = \sum_{l=1}^{M-1} \widetilde{\dot{z}_l^{n+1}} \sin\left(\frac{jl\pi}{M}\right), \tag{2.10}$$

where

$$\begin{aligned}
\widetilde{z_l^{n+1}} &= \cos(\theta_l\tau)\widetilde{z_l^n} + \frac{\sin(\theta_l\tau)}{\theta_l}\widetilde{\dot{z}_l^n} - \frac{\theta_l\tau}{2}\sin(\theta_l\tau)\widetilde{f_l^n},\\
\widetilde{\dot{z}_l^{n+1}} &= -\theta_l\sin(\theta_l\tau)\widetilde{z_l^n} + \cos(\theta_l\tau)\widetilde{\dot{z}_l^n} - \frac{\theta_l^2\tau}{2}\left[\cos(\theta_l\tau)\widetilde{f_l^n} + \widetilde{f_l^{n+1}}\right],
\end{aligned} \tag{2.11}$$

with

$$\begin{aligned}
\widetilde{z_l^n} &= \frac{2}{M}\sum_{j=1}^{M-1} z_j^n \sin\left(\frac{jl\pi}{M}\right), \quad \widetilde{\dot{z}_l^n} = \frac{2}{M}\sum_{j=1}^{M-1} \dot{z}_j^n \sin\left(\frac{jl\pi}{M}\right),\\
\widetilde{f_l^n} &= \frac{2}{M}\sum_{j=1}^{M-1} f(z_j^n)\sin\left(\frac{jl\pi}{M}\right).
\end{aligned}$$

The scheme is explicit and very efficient due to the fast discrete sine transform. The memory cost is $O(M)$ and the computational cost per time step is $O(M \ln M)$. We remark here that a Deuflhard-type exponential integrator Fourier/cosine pseudospectral scheme can be derived if the homogeneous boundary condition here is replaced by periodic/homogeneous Neumann boundary condition.

3 Error estimates

In this section, we give the convergence theorem for the fully discretized scheme (2.11). We denote $H^m(\Omega)$ by the standard Sobolev space. Introduce its subspace as

$$\widetilde{H}^m(\Omega) = \{u \in H^m(\Omega) : u^{(2k)}(a) = u^{(2k)}(b) = 0, \quad k \in \mathbb{N}, \quad 0 \le 2k < m\},$$

for some integer $m \ge 1$. For any function $u(x) = \sum_{l=1}^{\infty} \widehat{u}_l \sin(\mu_l(x-a)) \in \widetilde{H}^m(\Omega)$, we define its norm as

$$\|u\|_m^2 = \sum_{l=1}^{\infty} (1 + |\mu_l|^2)^m |\widehat{u}_l|^2. \tag{3.1}$$

It can be clearly seen that the norm $\|\cdot\|_m$ is equivalent to the classical Sobolev norm in the space H^m. Particularly, for $m = 0$, the space is exactly $L^2(\Omega)$ and the corresponding norm is denoted as $\|\cdot\|$.

For simplicity of notation, we denote the interpolations of the numerical solutions by

$$z_I^n(x) = I_M(z^n)(x), \quad \dot{z}_I^n(x) = I_M(\dot{z}^n)(x), \quad x \in (a, b),$$

and the error functions by

$$e^n(x) = z(x, t_n) - z_I^n(x), \quad \dot{e}^n(x) = \partial_t z(x, t_n) - \dot{z}_I^n(x), \quad x \in (a, b).$$

In order to obtain the convergence of the fully discrete scheme, we need the following auxiliary lemmas.

Lemma 3.1 [34] *For any $0 \le \mu \le k$ with $k > 1/2$, there exists a constant C such that*

$$\|u - P_M u\|_\mu \le C h^{k-\mu} \|u\|_k, \quad \|u - I_M u\|_\mu \le C h^{k-\mu} \|u\|_k, \quad \forall u \in \widetilde{H}^k(\Omega). \tag{3.2}$$

Lemma 3.2 [10] *For any function $g \in C^\infty(\mathbb{C}, \mathbb{C})$ and $\sigma > 1/2$, there exists a nondecreasing function $\chi_g : \mathbb{R}^+ \to \mathbb{R}^+$ such that*

$$\|g(u)\|_\sigma \le \|g(0)\|_\sigma + \chi_g(\|u\|_{L^\infty})\|u\|_\sigma, \quad \forall u \in H^\sigma. \tag{3.3}$$

For all $v, w \in B_R^\sigma := \{u \in H^\sigma : \|u\|_\sigma \le R\}$, we have

$$\|g(v) - g(w)\|_\sigma \le \alpha(g, R)\|v - w\|_\sigma, \tag{3.4}$$

where $\alpha(g, R) = \|g'(0)\|_\sigma + R\chi_{g'}(cR)$ is nondecreasing with respect to R, with $c > 0$ being the constant for the Sobolev imbedding $\|\cdot\|_{L^\infty} \le c\|\cdot\|_\sigma$.

Theorem 3.1 *Let the solution of the GIBq equation (2.1) satisfy the regularity properties* $z \in C^1([0,T];\widetilde{H}^{m+\sigma}) \cap C^2([0,T];\widetilde{H}^m)(m > 1/2, \sigma > 0)$. *Then there exist* $h_0 > 0$, $\tau_0 > 0$ *such that when* $\tau \le \tau_0$ *and* $h \le h_0$, *the numerical solutions* z^n *and* $\dot{z}^n$ *obtained from the DEI-SP scheme (2.10)–(2.11) converge to the solution of the problem (2.1) with the convergence rate*

$$\|e^n\|_m + \|\dot{e}^n\|_m \le C(f,T,K_1,K_2,K_3)\tau^2 + C(f,T,R_1,R_2)h^\sigma, \quad n = 0,1,\ldots,N, \tag{3.5}$$

where $K_i := \|\partial_t^{i-1} z\|_{L^\infty([0,T];H^m)}$ $(i = 1,2,3)$ *and* $R_i := \|\partial_t^{i-1} z\|_{L^\infty([0,T];H^{m+\sigma})}$ $(i = 1,2)$. *Furthermore, we have*

$$\|z_I^n\|_m \le K_1 + 1, \quad \|\dot{z}_I^n\|_m \le K_2 + 1. \tag{3.6}$$

Proof We give the proof for (3.5) and (3.6) by induction. For $n = 0$, noticing that $e^0 = z_0 - I_M(z_0)$, $\dot{e}^0 = z_1 - I_M(z_1)$, applying Lemma 3.1, one gets

$$\|e^0\|_m + \|\dot{e}^0\|_m \le C(R_1,R_2)h^\sigma.$$

Hence triangle inequality gives (3.6) when $h \le h_1 = 1/C(R_1,R_2)$, which completes the proof of (3.5) and (3.6) for $n = 0$. Assume (3.5) and (3.6) are true for $n \le k < T/\tau$, next we show that (3.5) and (3.6) are valid for $n = k+1$. For $n \ge 1$, denote

$$e_M^n(x) = P_M(e^n(x)) = \sum_{l=1}^{M-1} \widehat{e_l^n} \sin(\mu_l(x-a)),$$
$$\dot{e}_M^n(x) = P_M(\dot{e}^n(x)) = \sum_{l=1}^{M-1} \widehat{\dot{e}_l^n} \sin(\mu_l(x-a)),$$

by the projected error functions, where the corresponding coefficients in the frequency satisfy

$$\widehat{e_l^n} = \widehat{z_l}(t_n) - \widetilde{z_l^n}, \qquad \widehat{\dot{e}_l^n} = \widehat{z_l}'(t_n) - \widetilde{\dot{z}_l^n}.$$

By the triangle inequality and Lemma 3.1,

$$\begin{aligned}\|e^n\|_m + \|\dot{e}^n\|_m &\le \|e_M^n\|_m + \|\dot{e}_M^n\|_m + \|z(\cdot,t_n) - P_M(z(\cdot,t_n))\|_m \\ &\quad + \|\partial_t z(\cdot,t_n) - P_M(\partial_t z(\cdot,t_n))\|_m \\ &\le \|e_M^n\|_m + \|\dot{e}_M^n\|_m + C(R_1,R_2)h^\sigma,\end{aligned} \tag{3.7}$$

it suffices to show

$$\|e_M^n\|_m + \|\dot{e}_M^n\|_m \le C(\tau^2 + h^\sigma). \tag{3.8}$$

Denote the local truncation errors by

$$\xi^n(x) = \sum_{l=1}^{M-1} \widehat{\xi_l^n} \sin(\mu_l(x-a)), \qquad \dot{\xi}^n(x) = \sum_{l=1}^{M-1} \widehat{\dot{\xi}_l^n} \sin(\mu_l(x-a)), \tag{3.9}$$

where

$$\begin{aligned}
\widehat{\xi_l^n} &= \widehat{z_l}(t_{n+1}) - \cos(\theta_l\tau)\widehat{z_l}(t_n) - \frac{\sin(\theta_l\tau)}{\theta_l}\widehat{z_l}'(t_n) + \frac{\theta_l\tau}{2}\sin(\theta_l\tau)\widehat{f_l^n}(0),\\
\widehat{\dot{\xi}_l^n} &= \widehat{z_l}'(t_{n+1}) + \theta_l\sin(\theta_l\tau)\widehat{z_l}(t_n) - \cos(\theta_l\tau)\widehat{z_l}'(t_n)\\
&\quad + \frac{\theta_l^2\tau}{2}\left[\cos(\theta_l\tau)\widehat{f_l^n}(0) + \widehat{f_l^n}(\tau)\right],
\end{aligned} \tag{3.10}$$

with $\widehat{f_l^n}(s) = f(\widehat{z(t_n+s)})_l$. Subtracting (2.11) from (3.10), we have

$$\begin{aligned}
\widehat{e_l^{n+1}} &= \cos(\theta_l\tau)\widehat{e_l^n} + \frac{\sin(\theta_l\tau)}{\theta_l}\widehat{\dot{e}_l^n} + \widehat{\xi_l^n} - \frac{\theta_l\tau}{2}\sin(\theta_l\tau)\widehat{\eta_l^n},\\
\widehat{\dot{e}_l^{n+1}} &= -\theta_l\sin(\theta_l\tau)\widehat{e_l^n} + \cos(\theta_l\tau)\widehat{\dot{e}_l^n} + \widehat{\dot{\xi}_l^n} - \frac{\theta_l^2\tau}{2}\left(\cos(\theta_l\tau)\widehat{\eta_l^n} + \widehat{\eta_l^{n+1}}\right),
\end{aligned} \tag{3.11}$$

where $\widehat{\eta_l^n} = \widehat{f_l^n}(0) - \widetilde{f_l^n}$. Inserting (2.9) into (3.10) yields

$$\begin{aligned}
\widehat{\xi_l^n} &= -\theta_l\int_0^\tau \widehat{f_l^n}(w)\sin(\theta_l(\tau-w))dw + \frac{\theta_l\tau}{2}\sin(\theta_l\tau)\widehat{f_l^n}(0),\\
\widehat{\dot{\xi}_l^n} &= -\theta_l^2\int_0^\tau \widehat{f_l^n}(w)\cos(\theta_l(\tau-w))dw + \frac{\theta_l^2\tau}{2}\left[\cos(\theta_l\tau)\widehat{f_l^n}(0) + \widehat{f_l^n}(\tau)\right].
\end{aligned}$$

Note that the error formula of the trapezoidal rule for the function $g \in C^2[0,\tau]$ is given by

$$\int_0^\tau g(s)ds - \frac{\tau}{2}[g(0)+g(\tau)] = -\frac{1}{2}\int_0^\tau g''(s)s(\tau-s)ds. \tag{3.12}$$

It follows that

$$\begin{aligned}
\widehat{\xi_l^n} &= \frac{\theta_l}{2}\int_0^\tau s(\tau-s)[\sin(\theta_l(\tau-s))\widehat{f_l^n}(s)]''ds = \frac{\theta_l}{2}\int_0^\tau s(\tau-s)P_l^n(s)ds,\\
\widehat{\dot{\xi}_l^n} &= \frac{\theta_l^2}{2}\int_0^\tau s(\tau-s)[\cos(\theta_l(\tau-s))\widehat{f_l^n}(s)]''ds = \frac{\theta_l^2}{2}\int_0^\tau s(\tau-s)Q_l^n(s)ds,
\end{aligned}$$

where

$$P_l^n(s) = -\theta_l^2\sin(\theta_l(\tau-s))\widehat{f_l^n}(s) - 2\theta_l\cos(\theta_l(\tau-s))(\widehat{f_l^n})'(s) + \sin(\theta_l(\tau-s))(\widehat{f_l^n})''(s),$$

$$Q_l^n(s) = -\theta_l^2 \cos(\theta_l(\tau - s))\widehat{f_l^n}(s) + 2\theta_l \sin(\theta_l(\tau - s))(\widehat{f_l^n})'(s) + \cos(\theta_l(\tau - s))(\widehat{f_l^n})''(s).$$

Applying the Hölder's inequality and Minkowski's inequality, we get

$$\begin{aligned}
|\widehat{\xi_l^n}| &\le \frac{\theta_l}{2}\Big(\int_0^\tau s^2(\tau - s)^2 ds\Big)^{1/2}\Big(\int_0^\tau |P_l^n(s)|^2 ds\Big)^{1/2} \le \tau^{5/2}\Big(\int_0^\tau |P_l^n(s)|^2 ds\Big)^{1/2} \\
&\le C\tau^{5/2}\Big[\Big(\int_0^\tau |\widehat{f_l^n}(s)|^2\Big)^{1/2} + \Big(\int_0^\tau |(\widehat{f_l^n})'(s)|^2\Big)^{1/2} + \Big(\int_0^\tau |(\widehat{f_l^n})''(s)|^2\Big)^{1/2}\Big], \\
|\widehat{\dot{\xi}_l^n}| &\le \frac{\theta_l^2}{2}\Big(\int_0^\tau s^2(\tau - s)^2 ds\Big)^{1/2}\Big(\int_0^\tau |Q_l^n(s)|^2 ds\Big)^{1/2} \le \tau^{5/2}\Big(\int_0^\tau |Q_l^n(s)|^2 ds\Big)^{1/2} \\
&\le C\tau^{5/2}\Big[\Big(\int_0^\tau |\widehat{f_l^n}(s)|^2\Big)^{1/2} + \Big(\int_0^\tau |(\widehat{f_l^n})'(s)|^2\Big)^{1/2} + \Big(\int_0^\tau |(\widehat{f_l^n})''(s)|^2\Big)^{1/2}\Big].
\end{aligned}$$

Thus by using Lemma 3.2, the bilinear inequality [1]

$$\|vw\|_\sigma \le C\|v\|_\sigma \|w\|_\sigma, \quad \sigma > 1/2,$$

we get

$$\begin{aligned}
\|\xi^n\|_m^2 + \|\dot{\xi}^n\|_m^2 &= \sum_{l=1}^{M-1}(1 + \mu_l^2)^m(|\widehat{\xi_l^n}|^2 + |\widehat{\dot{\xi}_l^n}|^2) \\
&\le C\tau^5 \int_0^\tau \sum_{l=1}^{M-1}(1 + \mu_l^2)^m \Big(|(\widehat{f_l^n})(s)|^2 + |(\widehat{f_l^n})'(s)|^2 + |(\widehat{f_l^n})''(s)|^2\Big) ds \\
&\le C\tau^5 \int_0^\tau \Big[\|f(z(t_n + s))\|_m^2 + \|f'(z(t_n + s))\partial_t z(t_n + s)\|_m^2 \\
&\quad + \|f''(z(t_n + s))(\partial_t z(t_n + s))^2\|_m^2 + \|f'(z(t_n + s))\partial_{tt} z(t_n + s)\|_m^2\Big] ds \\
&\le C\tau^5 \int_0^\tau \Big[(\chi_f(\|z(t_n + s)\|_\infty))^2\|z(t_n + s)\|_m^2 + \|f'(z(t_n + s))\|_m^2\|\partial_t z(t_n + s)\|_m^2 \\
&\quad + \|f''(z(t_n + s))\|_m^2\|\partial_t z(t_n + s)\|_m^4 + \|f'(z(t_n + s))\|_m^2\|\partial_{tt} z(t_n + s)\|_m^2\Big] ds \\
&\le C(f, K_1, K_2, K_3)\tau^6. \qquad (3.13)
\end{aligned}$$

Multiplying the equations in (3.11) on both sides by themselves and applying the Cauchy's inequality, we get that

$$\begin{aligned}
&\theta_l^2\left|\widehat{e_l^{n+1}}\right|^2 + \left|\widehat{\dot{e}_l^{n+1}}\right|^2 \\
&\le (1 + \tau)\left|\theta_l \cos(\theta_l\tau)\widehat{e_l^n} + \sin(\theta_l\tau)\widehat{\dot{e}_l^n}\right|^2 + (1 + \frac{1}{\tau})\theta_l^2\left|\widehat{\xi_l^n} - \frac{\theta_l\tau}{2}\sin(\theta_l\tau)\widehat{\eta_l^n}\right|^2 \\
&\quad + (1 + \tau)\left|-\theta_l \sin(\theta_l\tau)\widehat{e_l^n} + \cos(\theta_l\tau)\widehat{\dot{e}_l^n}\right|^2
\end{aligned}$$

$$+\left(1+\frac{1}{\tau}\right)\left|\dot{\widehat{\xi}}_l^n-\frac{\theta_l^2\tau}{2}(\cos(\theta_l\tau)\widehat{\eta}_l^n+\widehat{\eta_l^{n+1}})\right|^2$$
$$\le(1+\tau)\left[\theta_l^2|\widehat{e_l^n}|^2+|\dot{\widehat{e}}_l^n|^2\right]+\left(1+\frac{1}{\tau}\right)\left[2\theta_l^2|\widehat{\xi}_l^n|^2+2|\dot{\widehat{\xi}}_l^n|^2+\theta_l^4\tau^2(|\widehat{\eta}_l^n|^2+|\widehat{\eta_l^{n+1}}|^2)\right].$$

Denote

$$\mathscr{E}^n=\sum_{l=1}^{M-1}(1+\mu_l^2)^m(\theta_l^2|\widehat{e_l^n}|^2+|\dot{\widehat{e}}_l^n|^2). \tag{3.14}$$

Noticing that $\theta_l\le 1$ and $\theta_l\ge\theta_1=\frac{\pi}{\sqrt{\pi^2+(b-a)^2}}$, this implies that

$$\mathscr{E}^{n+1}-\mathscr{E}^n\le\tau\mathscr{E}^n+2\left(1+\frac{1}{\tau}\right)\left(\|\xi^n\|_m^2+\|\dot{\xi}^n\|_m^2\right)+\tau^2\left(1+\frac{1}{\tau}\right)(\|\eta^n\|_m^2+\|\eta^{n+1}\|_m^2), \tag{3.15}$$

where

$$\eta^n(x)=\sum_{l=1}^{M-1}\widehat{\eta}_l^n\sin(\mu_l(x-a)).$$

By induction (3.6), we clearly see that $z_I^n, z(\cdot,t_n)\in B_{K_1+1}^m$. Employing (3.3) and (3.4), we get

$$\begin{aligned}\|\eta^n\|_m&=\|I_M(f(z_I^n))-P_M(f(z(\cdot,t_n)))\|_m\\&\le\|I_M(f(z_I^n)-f(z(\cdot,t_n)))\|_m+\|I_M(f(z(\cdot,t_n)))-P_M(f(z(\cdot,t_n)))\|_m\\&\le C\|f(z_I^n))-f(z(\cdot,t_n))\|_m+Ch^\sigma\|f(z(\cdot,t_n))\|_{m+\sigma}\\&\le C\alpha(f,K_1+1)\|z_I^n-z(\cdot,t_n)\|_m+Ch^\sigma\chi_f(\|z(\cdot,t_n)\|_{L^\infty})\|z(\cdot,t_n)\|_{m+\sigma}\\&\le C\alpha(f,K_1+1)[(\mathscr{E}^n)^{1/2}+h^\sigma R_1]+Ch^\sigma\chi_f(cK_1)R_1,\end{aligned}$$

which implies that

$$\|\eta^n\|_m^2\le C(f,K_1)\mathscr{E}^n+C(f,R_1)h^{2\sigma}.$$

Next we show that z_I^{n+1} is bounded in H^m. It follows from (2.11), the induction (3.6) and (3.3) that

$$\begin{aligned}\|z_I^{n+1}\|_m&\le\|z_I^n\|_m+\|\dot{z}_I^n\|_m+\tau/2\|I_M(f(z_I^n))\|_m\\&\le K_1+K_2+2+C\tau\|f(z_I^n)\|_m\\&\le K_1+K_2+2+C\tau\chi_f(c\|z_I^n\|_m)\|z_I^n\|_m\le C(f,K_1,K_2).\end{aligned}$$

Hence similarly we have

$$\|\eta^{n+1}\|_m^2 \le C(f, K_1, K_2)\mathscr{E}^{n+1} + C(f, K_2, R_1)h^{2\sigma}.$$

This together with (3.15) and (3.13) yields that

$$\begin{aligned}&\mathscr{E}^{n+1} - \mathscr{E}^n\\ &\quad\le \tau\mathscr{E}^n + C(f, K_1, K_2, K_3)\tau^5 + \tau C(f, K_1, K_2)(\mathscr{E}^n + \mathscr{E}^{n+1}) + \tau C(f, K_2, R_1)h^{2\sigma}.\end{aligned}$$

Summing the above inequality for $n = 0, 1, \ldots, k$, one yields

$$\mathscr{E}^{k+1} - \mathscr{E}^0 \le C(f, K_1, K_2, K_3)\tau^4 + C(f, K_2, R_1)h^{2\sigma} + \tau C(f, K_1, K_2)\sum_{n=0}^{k+1}\mathscr{E}^n.$$

Noticing that

$$\mathscr{E}^0 \le \|e_M^0\|_m^2 + \|\dot{e}_M^0\|_m^2 \le C(R_1, R_2)h^{2\sigma} + \|e^0\|_m^2 + \|\dot{e}^0\|_m^2 \le C(R_1, R_2)h^{2\sigma},$$

we derive when $\tau \le \tau_1 = \frac{1}{2C(f,K_1,K_2)}$,

$$\mathscr{E}^{k+1} \le C(f, K_1, K_2, K_3)\tau^4 + C(f, K_2, R_1)h^{2\sigma} + \tau C(f, K_1, K_2)\sum_{n=0}^{k}\mathscr{E}^n.$$

Using the discrete Gronwall's inequality, we get

$$\mathscr{E}^{k+1} \le C(f, T, K_1, K_2, K_3)\tau^4 + C(f, T, R_1, K_2)h^{2\sigma}.$$

Recalling the definition of $\mathscr{E}^n$ [cf. (3.14)], one immediately derives (3.8). Finally (3.5) can be obtained by (3.7). Setting $\tau_0 = \min\{\tau_1, 1/\sqrt{2C(f, T, K_1, K_2, K_3)}\}$, $h_0 = \min\{h_1, 1/(2C(f, T, R_1, R_2))^{1/2\sigma}\}$, then (3.6) is established by the triangle inequality and (3.5) when $h \le h_0$ and $\tau \le \tau_0$. The proof is completed. □

Remark 3.1 As is seen from Theorem 3.1, the DEI-SP method is convergent without any CFL-type condition required, although it is fully explicit. This could be understood as follows. As is similar to the Klein-Gordon equation, in which case the Deuflhard-type exponential integrator is equivalent to a time-splitting method for temporal approximations [29,34], here the proposed DEI-SP scheme (2.10)–(2.11) can also be derived from a time-splitting pseudospectral discretization approach. Specifically, denote $v = z_t$, then the GIBq equation can be written as a first-order system

$$\begin{cases} z_t(x,t) = v(x,t),\\ v_t(x,t) - v_{txx}(x,t) = z_{xx}(x,t) + (f(z))_{xx}(x,t),\\ z(x,0) = z_0(x), \quad v(x,0) = z_1(x).\end{cases}$$

We decompose it into the following two subproblems

$$A:\begin{cases} z_t(x,t)=v(x,t), \\ v_t(x,t)-v_{txx}(x,t)=z_{xx}(x,t), \\ z(x,0)=z_0(x), \quad v(x,0)=z_1(x), \end{cases} \qquad B:\begin{cases} z_t(x,t)=0, \\ v_t(x,t)-v_{txx}(x,t)=(f(z))_{xx}(x,t), \\ z(x,0)=z_0(x), \quad v(x,0)=z_1(x). \end{cases}$$

Then the linear problem A can be solved exactly in phase space and the corresponding evolution operator is denoted by $\begin{pmatrix} z(\cdot,t) \\ v(\cdot,t) \end{pmatrix} = \chi_A^t \begin{pmatrix} z_0 \\ z_1 \end{pmatrix}$. Similarly, the nonlinear problem B can also be integrated exactly in phase space due to the fact that $z(x,t)$ keeps invariant and denote the associated evolution operator by $\begin{pmatrix} z(\cdot,t) \\ v(\cdot,t) \end{pmatrix} = \chi_B^t \begin{pmatrix} z_0 \\ z_1 \end{pmatrix}$. By using the second-order Strang splitting $\chi_B^{\tau/2}\chi_A^{\tau}\chi_B^{\tau/2}$ combined with the spectral discretization in space, we arrive at the same numerical scheme as (2.11). Noticing that each subproblem is integrated exactly in phase space, this enables the CFL-type condition to be exempted.

4 Numerical experiments

In this section, we firstly show some numerical results to testify the accuracy of the proposed DEI-SP method and compare the numerical results to those of other methods in the literature. Then the method is applied to investigate long time dynamics of the GIBq equation, e.g., propagation of a single solitary wave, interaction of two solitary waves. For all the numerical experiments, we choose the commonly used nonlinearity $f(u)=u^p$ with $p=2$ or $p=3$.

4.1 Accuracy test

In this subsection we present some numerical results to confirm the convergence and compare our method with some other methods proposed in the literature. Denote $z_{\tau,h}$ and $\dot{z}_{\tau,h}$ by the numerical solutions obtained by the DEI-SP method with time step τ and mesh size h. To quantify the numerical error, we define the error function as

$$e_{\tau,h} := \|I_M(z_{\tau,h}) - z(\cdot,t)\|_1 + \|I_M(\dot{z}_{\tau,h}) - \partial_t z(\cdot,t)\|_1.$$

Example 1 Solitary wave solutions of the generalized GIBq equation are given in the form [3,20,26]

$$z(x,t) = A\,\mathrm{sech}^{\frac{2}{p-1}}\Big(\frac{p-1}{2c}\sqrt{c^2-1}(x-x_0-ct)\Big), \quad c=\pm\sqrt{\frac{1+2A^{p-1}}{p+1}}, \tag{4.1}$$

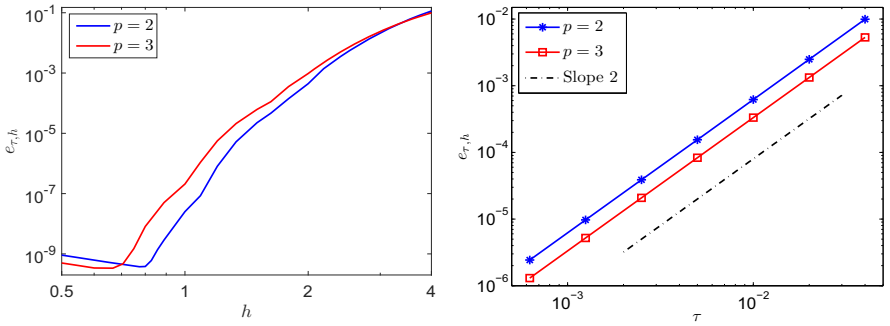

Fig. 1 Spatial (left) and temporal (right) errors of the DEI-SP scheme for the soliton solution under different mesh size and time step size

where A is the amplitude and c is the velocity of the pulse centered at x_0 initially with $c^2 > 1$. Noticing that the solitary wave decays drastically in the far field, this enables us to approach the GIBq equation on a bounded interval $\Omega = (a, b)$ with zero boundary conditions when $|a|$ and b are sufficiently large. Here we choose $A = 1/2$, $x_0 = 0$ and the domain $\Omega = (-300, 300)$.

Figure 1 displays the spatial and temporal errors of the DEI-SP method (2.10)–(2.11) for the solitary wave solution with $p = 2$ and $p = 3$ at $t = 5$ under different choices of τ and h. To testify the spatial accuracy, we take a tiny time step $\tau = 5.0E-5$ such that the temporal error is negligible; for temporal error analysis, we set the mesh size $h = 1/8$ such that the spatial error can be ignorable. It can be clearly observed that the scheme converges quadratically in time, which agrees with the theoretical result in Theorem 3.1. For spatial convergence, the error decays very rapidly when the number of grid points increases and then saturates when temporal discretization error dominates. This suggests that the method converges spectrally in space, which coincides with the analysis in Theorem 3.1.

Next we investigate the long time behavior of the DEI-SP method. Figure 2 shows the difference of mass (1.3) for the numerical solitary wave solution (left) and the long time error of the DEI-SP scheme (right), where the computations are performed on the domain $\Omega = (-300, 300)$ with $h = 1/8$ and $\tau = 0.001$ and the integral $\mathscr{M}(t)$ (1.3) is approximated by Simpson's quadrature. It can be clearly observed that although the DEI-SP method fails to satisfy the mass conservation law exactly, it preserves the mass very well, even for long time dynamics. On the other hand, the right plot of Fig. 2 shows that the error increases mildly and almost linearly with respect to time, which together with the left plot suggests that the DEI-SP method is reliable for long time dynamics.

For a comparison with other numerical methods, we choose the quadratic nonlinearity ($p = 2$), and the corresponding initial conditions of the solitary wave solution (4.1) with different A as were used in literature [7,8,16,25]. Table 1 displays the l^∞-errors of different numerical methods at $t = 72$ with the same mesh size $h = 0.1$ and time step $\tau = 0.001$. Here we compare the present DEI-SP method with the second-order implicit finite difference method (IFDM) [8], the predictor-corrector (P-C) scheme

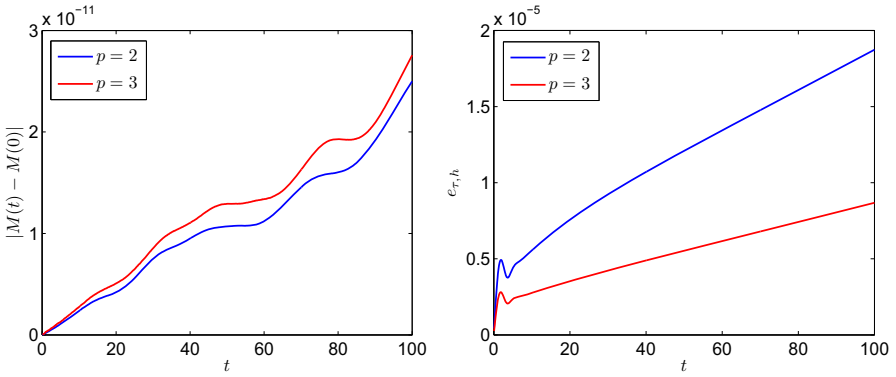

Fig. 2 Conservation of mass (left) and long-time errors of the DEI-SP method (right)

Table 1 Comparison of error for the DEI-SP method and other methods in literature

A	DEI-SP	RBFs [25]	M4 [16]	IFDM [8]	P-C [7]
0.25	1.53E–9	1.86E–7	1.80E–7	1.79E–4	–
0.5	1.42E–8	7.93E–7	7.50E–7	4.19E–4	4.19E–4
0.75	5.10E–8	1.88E–6	1.89E–6	2.90E–3	2.90E–3
0.9	8.99E–8	2.97E–6	2.96E–6	1.35E–2	1.35E–2

Table 2 Comparison of efficiency between the DEI-SP method and other methods in literature

A	DEI-SP CPU time	RBFs [25] CPU time	IFDM [8] CPU time
0.25	203	3.29E+4	3.86E+4
0.5	201	3.35E+4	3.96E+4
0.75	202	3.36E+4	4.00E+4
0.9	201	3.32E+4	4.03E+4

[7], a variant of finite element method (M4) applied in [16] and a third-order meshless method based on collocation and approximating the solution by radial basis functions (RBFs) proposed in [25]. It can be clearly seen that our numerical method is much more accurate than those presented in [7,8,16]. DEI-SP method is even competitive with the third-order scheme [25], which is much time-consuming due to the iteration for solving a nonlinear system in each time step. We also compare the CPU time for some numerical methods with the same mesh size $h = 0.1$ and time step $\tau = 0.001$ in Table 2, where we compute till $t = 72$. The numerical comparison suggests that our DEI-SP scheme is much more efficient.

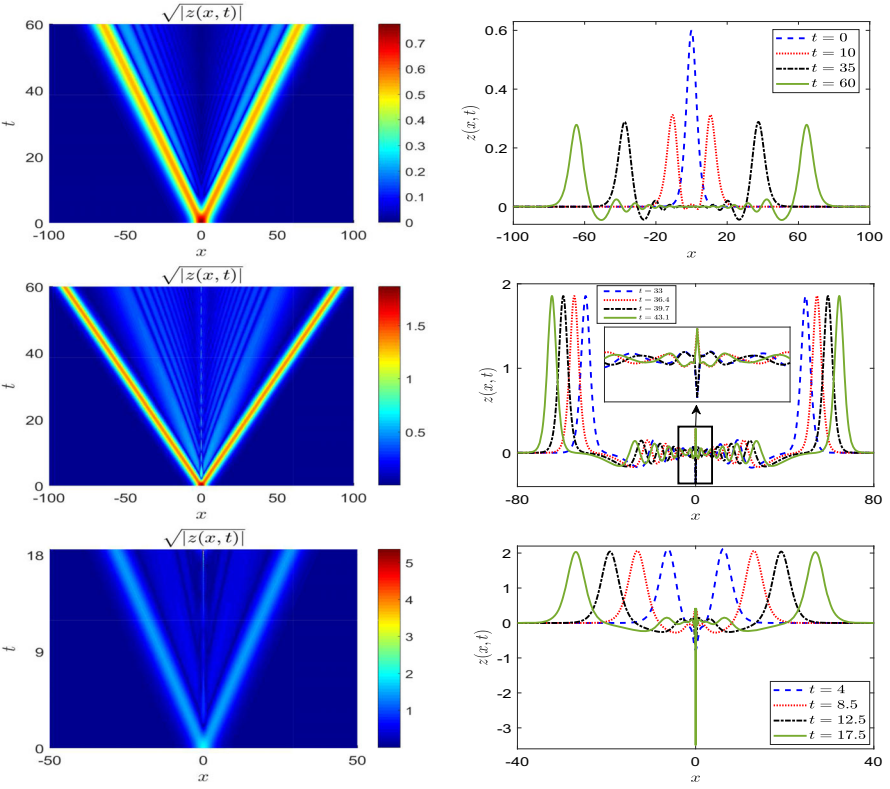

Fig. 3 Time evolution of the static solitary wave (4.2) for different A: $A = 0.6, 3.5, 3.8$ (from top to bottom)

4.2 Single-wave splitting

Example 2 In this experiment, we use the initial data for $p = 2$:

$$z_0(x) = A\,\mathrm{sech}^2\Big(\sqrt{\frac{A}{6}}\frac{x - x_0}{c}\Big), \quad z_1(x) = 0, \quad c = \sqrt{1 + \frac{2A}{3}}, \tag{4.2}$$

and $p = 3$:

$$z_0(x) = A\,\mathrm{sech}\Big(\frac{A}{\sqrt{2}}\frac{x - x_0}{c}\Big), \quad z_1(x) = 0, \quad c = \sqrt{1 + \frac{A^2}{2}}, \tag{4.3}$$

which has ever been applied for studying the single-wave splitting for $p = 2$ in the literature [28,33]. For both sets of initial data, computations are carried out with $h = 1/8$ and $\tau = 0.001$ on the interval $\Omega = (-400, 400)$.

Figure 3 displays the dynamics of the soliton with null initial velocity and different amplitudes $A = 0.6, 3.5, 3.8$ for $p = 2$ [cf. (4.2)]. We find that the soliton splits into

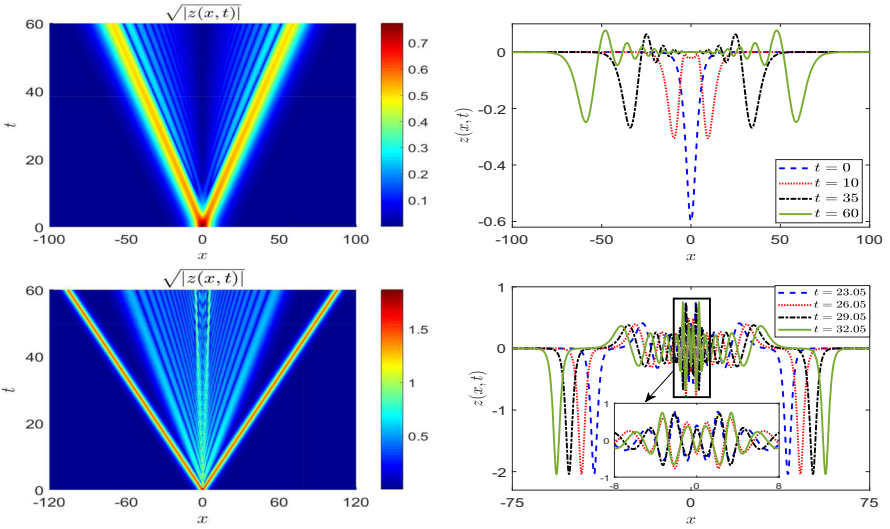

Fig. 4 Time evolution of the negative static solitary wave (4.3) for different A: $A = -0.6$ (above) and $A = -3.5$ (bellow)

two symmetric pulses moving in opposite directions. Besides the two main solitons, some oscillating tail is emitted between the two main waves, which is different from that of the "Good" Boussinesq equation where the emitting oscillations are beyond the main solitons [27]. From the figure for $A = 3.5$, we can see how the oscillations are emitted clearly. There is always a small pulse staying in the original location besides the splitting outspreading waves. As time evolves, the pulse oscillates up and down, breaks into new symmetric waves spreading outside in each period such that the amplitude of the pulse staying in the original site gets smaller and smaller. Furthermore, for soliton with initial amplitude large enough, the solution blows up in finite time, e.g., for $A = 3.8$, the solution blows up quickly after $t = 18.5$. Here blow-up means that the numerical solution goes to infinity quickly. For instance, for $A = 3.8$, when the computation is performed on $\Omega = (-400, 400)$ with $h = 1/8$ and $\tau = 0.001$, the solution goes to infinity at $t = 19$ exactly. When the computational domain is enlarged, the blow-up time is invariant. When the mesh size or time step is reduced, the exact blow-up time might change a little bit, for instance, when $h = 1/16$ and $\tau = 0.0001$, the blow-up phenomenon occurs at $t = 18.91$. Anyway, the computational parameters don't affect the blow-up property. By the way, this blow-up phenomena has not been revealed in e.g., [14,28,33].

Figure 4 displays the dynamics of the negative static soliton with different amplitudes $A = -0.6, -3.5$ for $p = 3$ (4.3). It can be observed that the dynamics is similar to the case for $p = 2$ when the amplitude is small. However, as the amplitude gets larger, the dispersion between the two main splitting waves gets more and more complicated (cf. Fig. 5). Furthermore, no finite time blow-up is found even for very large amplitude $A = -12$ (cf. Fig. 5), which is different from the case for $p = 2$ (cf. Fig. 3 bottom).

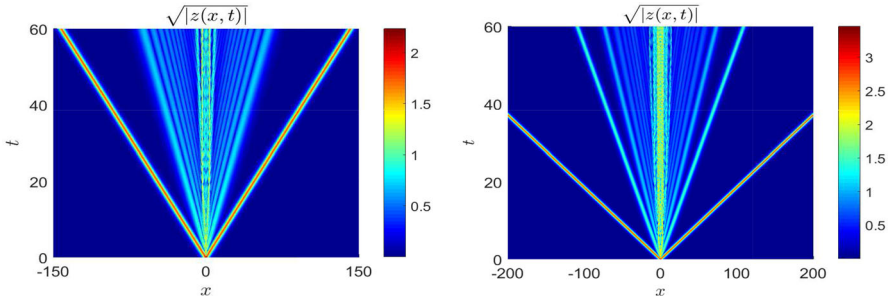

Fig. 5 Time evolution of the negative static solitary wave (4.3) for different A: $A = -5$ (left) and $A = -12$ (right)

4.3 Interaction of two solitary waves

In this subsection, we present some results to investigate the interaction of two solitary waves. The initial conditions are set as

$$\begin{aligned} z_0(x) &= \sum_{i=1}^{2} A_i \,\mathrm{sech}^{\frac{2}{p-1}}\Big(\frac{p-1}{2c_i}\sqrt{c_i^2-1}(x-x_i)\Big), \quad c_i = \pm\sqrt{1+2A_i^{p-1}/(p+1)}, \\ z_1(x) &= \sum_{i=1}^{2} A_i\sqrt{c_i^2-1}\,\mathrm{sech}^{\frac{2}{p-1}}\big(\frac{p-1}{2c_i}\sqrt{c_i^2-1}(x-x_i)\big)\tanh\big(\frac{p-1}{2c_i}\sqrt{c_i^2-1}(x-x_i)\big), \end{aligned} \tag{4.4}$$

with $p = 2$ or $p = 3$. It represents two solitary waves located initially at the positions $x = x_1$ and $x = x_2$, respectively, moving to the right or left depending on the sign of the velocity c_i. The experiments in this subsection are performed by the DEI-SP method over the interval $\Omega = (-400, 400)$ with $h = 1/8$ and $\tau = 0.001$.

Firstly we set $p = 2$ and consider the following cases for the initial data:
(1) *Inelastic collision* ($c_1 > 0, c_2 < 0$)*:*

(i) $x_1 = -x_2 = 40$, $A_1 = 0.2$, $A_2 = 0.3$;
(ii) $x_1 = -x_2 = 40$, $A_1 = 2.5$, $A_2 = 2$;

(2) *Blow-up phenomenon* ($c_1 > 0, c_2 < 0$)*:*

(iii) $x_1 = -x_2 = 40$, $A_1 = A_2 = 2.55$;
(iv) $x_1 = -x_2 = 40$, $A_1 = A_2 = 2.56$;
(v) $x_1 = -x_2 = 40$, $A_1 = 3.35$, $A_2 = 2$;
(vi) $x_1 = -x_2 = 40$, $A_1 = 3.36$, $A_2 = 2$;

(3) *Overtaking interaction* ($c_1 > 0, c_2 > 0$)*:*

(vii) $x_1 = -60$, $x_2 = -10$, $A_1 = 5$, $A_2 = 0.3$.

Figure 6 shows the evolution of $z(x, t)$ for *inelastic collision* [Cases (i)–(ii)]. We see that the two solitons which are initially located at the positions $x_1 = -40$ and $x_2 = 40$ moving towards each other with velocities c_1 and c_2, respectively. As time progresses

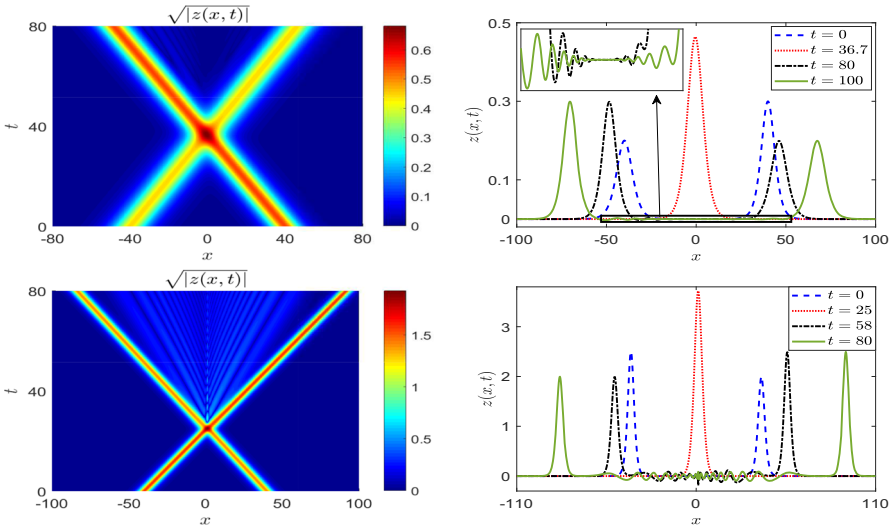

Fig. 6 Inelastic collision of two solitons for Cases (i)–(ii) (from top to bottom)

they collide, stick together and split after collision. Different from the discussions in most references [25,28,30], where the authors concluded that the collision is elastic when the initial amplitudes are small and inelastic collision occurs only when the maximum of the initial amplitudes is large, we'd prefer to say that the collision between two solitary waves for the GIBq equation is always inelastic, which means small radiation is created after the interaction. Specifically, for Case (i), the collision occurs at around $t = 36.7$ with the largest amplitude 0.4643, which is smaller than the summation of the two initial amplitudes. Small secondary waves are emitted after the interaction and can be seen clearly via a more careful observation. This small emission was ignored in the literature [25,28,30]. Furthermore, the collision here is completely different from the elastic collision for the "Good" Boussinesq equation [27], where the solitons retain their amplitudes and shape after the interaction and no displacement is observed.

Figure 7 reveals the *blow-up phenomenon* for the head-on collision. For two solitary waves with the same initial amplitude $A_1 = A_2 = A$, there exists $A_c \in (2.55, 2.56)$ such that the solution blows up in finite time when $A_1 = A_2 > A_c$. For $A_1 = A_2 = 2.56$, the solution blows up quickly after $t = 40$. Similar blow-up occurs for $x_1 = -x_2 = 10$, which means A_c does not depend on the relative locations of the initial solitons. For fixed $A_2 = 2$, there exists $A_c \in (3.35, 3.36)$ such that the solution blows up in finite time when $A_1 > A_c$. This suggests that there exists some instability for this kind of initial data. As far as we know, this blow-up phenomena after collision has never been investigated in literature.

Figure 8 shows the *overtaking interaction* of two solitons moving in the same direction with different velocities. It can be observed that the faster wave overtakes the slower one at around $t = 49.3$ with decreased amplitude and leaves it behind as time evolves. Furthermore, small waves are emitted during the overtaking process and

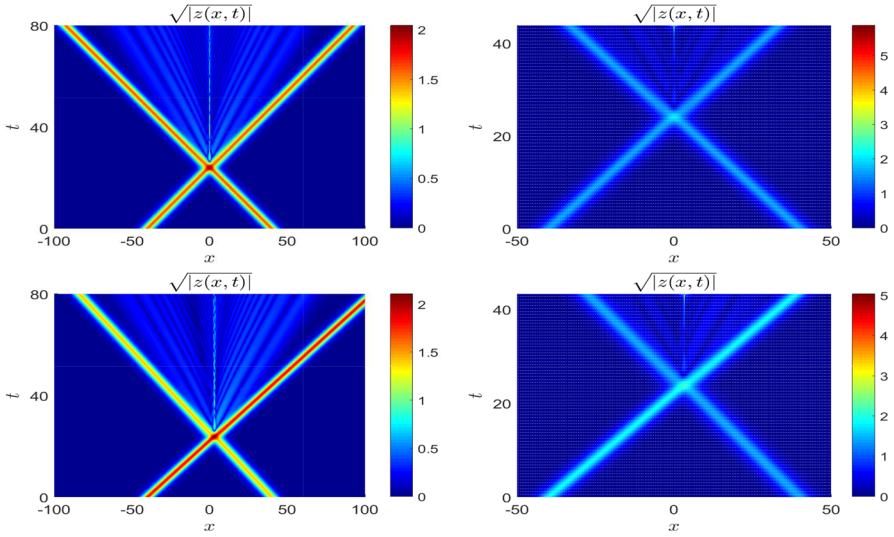

Fig. 7 Collision of two solitons for Cases (iii)–(vi) (from top to bottom, from left to right)

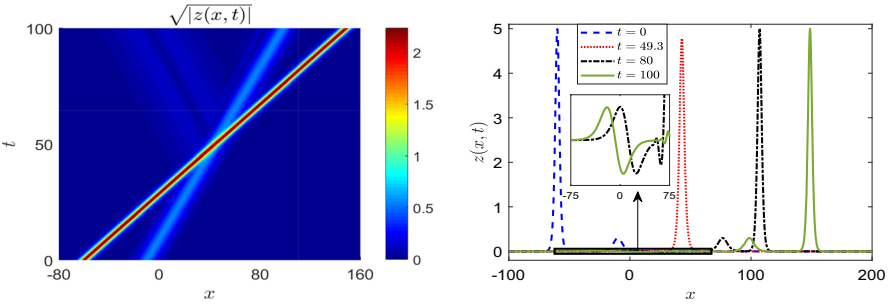

Fig. 8 Overtaking interaction of two solitons traveling in the same direction

some of these small waves propagate in the opposite direction, which is different from the case for the "Good" Boussinesq equation where no secondary waves are created during the interaction [27].

For $p = 3$, it is possible to choose negative A which corresponds to antisolitary waves. Next we investigate the interaction between solitary waves or between solitary and antisolitary waves for the GIBq equation with cubic nonlinearity ($p = 3$). We choose the following sets of initial conditions:

(1) *Inelastic collision* ($c_1 > 0, c_2 < 0$)*:*

(i) $x_1 = -x_2 = 40, A_1 = -0.2, A_2 = 0.3;$
(ii) $x_1 = -x_2 = 40, A_1 = 2.5, A_2 = -2;$
(iii) $x_1 = -x_2 = 40, A_1 = A_2 = 8;$
(iv) $x_1 = -x_2 = 40, A_1 = 12, A_2 = 5;$

(2) *Overtaking interaction* ($c_1 > 0, c_2 > 0$)*:*

(v) $x_1 = -60, x_2 = -10, A_1 = 5, A_2 = -2.$

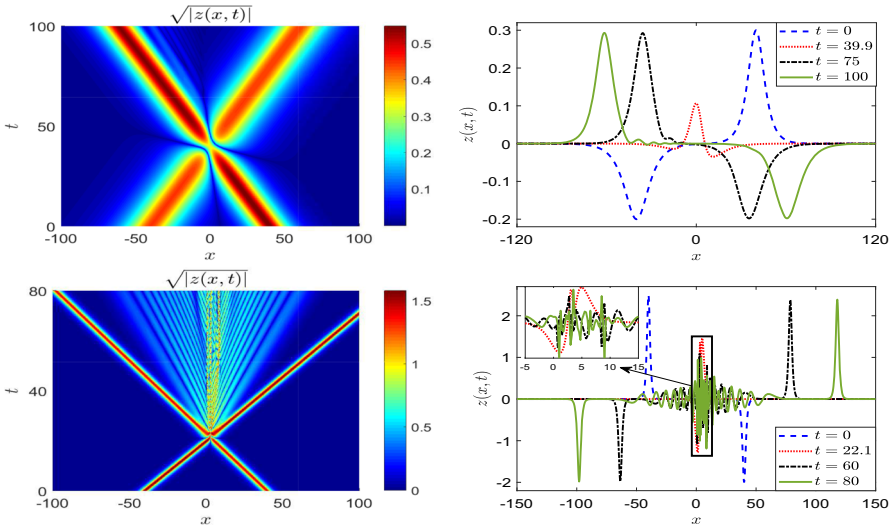

Fig. 9 Head-on collision between solitary and antisolitary waves for $p = 3$: Cases (i)–(ii) (from top to bottom)

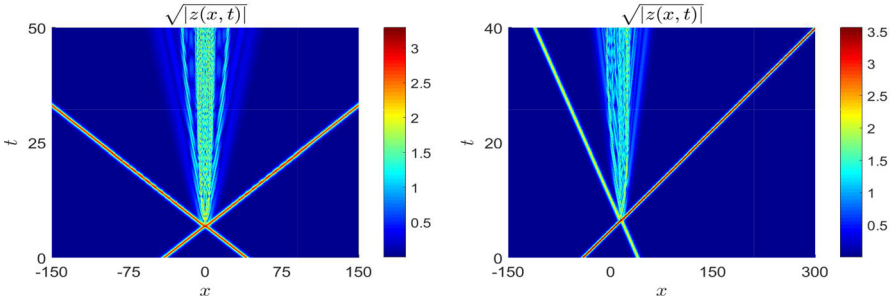

Fig. 10 Head-on collision between two solitons with large amplitudes for $p = 3$: Case (iii) (left) and Case (iv) (right)

Figure 9 shows the head-on interaction between solitary and antisolitary waves [Cases (i)–(ii)]. We see that the collision is inelastic and the interaction is similar to that of $p = 2$. For Case (i), the collision occurs at around $t = 39.9$ with the smallest amplitude 0.1068, which is larger than the difference of the initial amplitudes between the two original waves.

Figure 10 shows the head-on collision between two solitons with large amplitudes. Different from the case for $p = 2$ where blow-up occurs in finite time (cf. Fig. 7), no finite time explosion is found here, at least for solitary waves with initial amplitudes as large as $A_1 = A_2 = 8$ or $A_1 = 12$, $A_2 = 5$. However, the dynamics of the secondary emitting waves are definitely more and more complicated.

Figure 11 displays the *overtaking interaction* of a solitary wave and an antisolitary wave moving in the same direction with different velocities. Similarly, the faster wave overtakes the slower one and small solitary waves are emitted during the over-

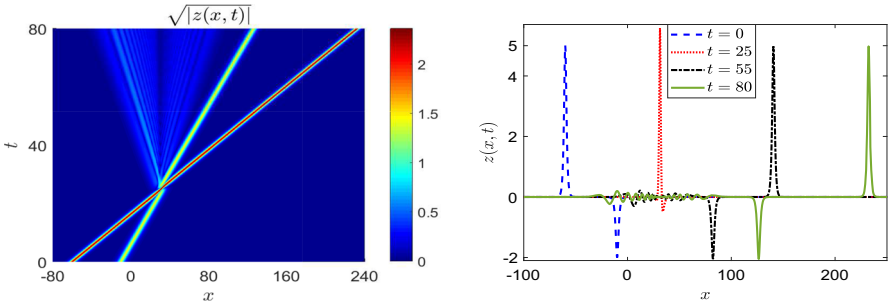

Fig. 11 Overtaking interaction of a solitary wave and an antisolitary wave for $p = 3$

taking interaction. Noticing that the overtaking takes place at around $t = 25$ with the maximum amplitude as $A = 5.5818$, which is different from the case when it occurs between two solitary or two antisolitary waves where the amplitude attains the minimum during the interaction.

5 Conclusions

A Deuflhard-type exponential integrator sine pseudospectral method was proposed for the generalized improved Boussinesq (GIBq) equation based on a sine pseudospectral discretization in space and a Dueflhard-type exponential integrator for time integration. The method was shown to unconditionally converge at the second order in time and spectrally in space. The convergence was confirmed by extensive numerical experiments. Comparison with other methods show its superiority in efficiency and accuracy. With this efficient method, some interesting numerical experiments are performed, e.g., *single-wave splitting*, *head-on/overtaking interaction* and *blow-up phenomena*. The numerical results suggest that there exists some essential difference on the dynamics of the GIBq equation with quadratic and cubic nonlinearities.

Acknowledgements C. Su is supported by the Alexander von Humboldt Foundation. C. Su would like to thank the Isaac Newton Institute for Mathematical Sciences for support and hospitality during the programme *Geometry, compatibility and structure preservation in computational differential equations* when work on this paper was taken. The second author would like to thank Dr. Ali Shokri for helpful communication.

References

1. Adams, R.A., Fournier, J.: Sobolev Spaces, vol. 140. Academic Press, Berlin (2003)
2. Berezin, Y.A., Karpman, V.I.: Nonlinear evolution of disturbances in plasmas and other dispersive media. Soviet Phys. JETP **24**, 1049–1055 (1967)
3. Bogolubsky, I.L.: Some examples of inelastic soliton interaction. Comput. Phys. Commun. **13**, 149–155 (1977)
4. Borluk, H., Muslu, G.M.: A Fourier pseudospectral method for a generalized improved Boussinesq equation. Numer. Methods Partial Differ. Equ. **31**, 995–1008 (2015)
5. Boussinesq, M.J.: Théorie de l'intumescence liquide, appelée onde solitaire ou de translation, se propageant dans un canal rectangulaire. CR Acad. Sci. Paris **72**, 755–759 (1871)

6. Boussinesq, M.J.: Théorie des ondes et des remous qui se propagent le long d'un canal rectangulaire horizontal, en communiquant au liquide contenu dans ce canal des vitesses sensiblement pareilles de la surface au fond. J. Math. Pures Appl. **17**, 5–108 (1872)
7. Bratsos, A.G.: A second order numerical scheme for the improved Boussinesq equation. Phys. Lett. A **370**, 145–147 (2007)
8. Bratsos, A.G.: A predictor–corrector scheme for the improved Boussinesq equation. Chaos Soliton Fract. **40**, 2083–2094 (2009)
9. Cerpa, E., Crépeau, E.: On the controllability of the improved Boussinesq equation. SIAM J. Control Optim. **56**, 3035–3049 (2018)
10. Chartier, Ph, Méhats, F., Thalhammer, M., Zhang, Y.: Improved error estimates for splitting methods applied to highly-oscillatory nonlinear Schrödinger equations. Math. Comput. **85**, 2863–2885 (2016)
11. Chen, G.W., Wang, S.B.: Existence and nonexistence of global solutions for the generalized IMBq equation. Nonlinear Anal. **36**, 961–980 (1999)
12. Christiansen, P.L., Muto, V., Soerensen, M.P.: Solitary waves on nonlinear elastic rods. North-Holland Ser. Appl. Math. Mech. **35**, 167–172 (1989)
13. Deuflhard, P.: A study of extrapolation methods based on multistep schemes without parasitic solutions. ZAMP **30**, 177–189 (1979)
14. El-Zoheiry, H.: Numerical study of the improved Boussinesq equation. Chaos Soliton Fract. **14**, 377–384 (2002)
15. Frutos, J.D., Ortega, T., Sanz-Serna, J.M.: Pseudospectral method for the good Boussinesq equation. Math. Comput. **57**, 109–122 (1991)
16. Irk, D., Dag, I.: Numerical simulations of the improved Boussinesq equation. Numer. Methods Partial Differ. Equ. **26**, 1316–1327 (2010)
17. Kishimoto, N.: Sharp local well-posedness for the "good" Boussinesq equation. J. Differ. Equ. **254**, 2393–2433 (2013)
18. Korteweg, D., De Vries, G.: On the change of form of long waves advancing in a rectangular channel, and a new type of long stationary wave. Phil. Mag. **39**, 422–443 (1895)
19. Lin, Q., Wu, Y.H., Loxton, R., Lai, S.: Linear B-spline finite element method for the improved Boussinesq equation. J. Comput. Appl. Math. **224**, 658–667 (2009)
20. Makhankov, V.G.: Dynamics of classical solitons (in non-integrable systems). Phys. Rep. **35**, 1–128 (1978)
21. Manoranjan, V.S., Mitchell, A.R., Morris, J.L.: Numerical solutions of the good Boussinesq equation. SIAM J. Sci. Comput. **5**, 946–957 (1984)
22. Mohebbi, A.: Solitary wave solutions of the nonlinear generalized Pochhammer–Chree and regularized long wave equations. Nonlinear Dyn. **70**, 2463–2474 (2012)
23. Oh, S., Stefanov, A.: Improved local well-posedness for the periodic "good" Boussinesq equation. J. Differ. Equ. **254**, 4047–4065 (2013)
24. Ostermann, A., Su, C.: Two exponential-type integrators for the "good" Boussinesq equation. Numer. Math. **143**, 683–712 (2019)
25. Shokri, A., Dehghan, M.: A not-a-knot meshless method using radial basis functions and predictor–corrector scheme to the numerical solution of improved Boussinesq equation. Comput. Phys. Commun. **181**, 1990–2000 (2010)
26. Soerensen, M.P., Christiansen, P.L., Lomdahl, P.S.: Solitary waves on nonlinear elastic rods I. J. Accoust. Soc. Am. **76**, 871–879 (1984)
27. Su, C., Yao, W.: A Deuflhard-type exponential integrator Fourier pseudo-spectral method for the "Good" Boussinesq equation. J. Sci. Comput. **83**, 4, (2020). https://doi.org/10.1007/s10915-020-01192-2
28. Wang, Q., Zhang, Z., Zhang, X., Zhu, Q.: Energy-preserving finite volume element method for the improved Boussinesq equation. J. Comput. Phys. **270**, 58–69 (2014)
29. Xu, Z., Dong, X., Zhao, X.: On time-splitting pseudospectral discretization for nonlinear Klein–Gordon equation in nonrelativistic limit regime. Commun. Comput. Phys. **16**, 440–466 (2014)
30. Yan, J., Zhang, Z., Zhao, T., Liang, D.: High-order energy-preserving schemes for the improved Boussinesq equation. Numer. Methods Partial Differ. Equ. **34**(4), 1145–1165 (2018)
31. Yang, Z.: Existence and non-existence of global solutions to a generalized modification of the improved Boussinesq equation. Math. Methods Appl. Sci. **21**, 1467–1477 (1988)
32. Yang, Z., Wang, X.: Blowup of solutions for improved Boussinesq type equation. J. Math. Anal. Appl. **278**, 335–353 (2003)

33. Zhang, Z., Lu, F.: Quadratic finite volume element method for improved Boussinesq equation. J. Math. Phys. **53**, 1–18 (2012)
34. Zhao, X.: On error estimates of an exponential wave integrator sine pseudospectral method for the Klein–Gordon–Zakharov system. Numer. Methods Partial Differ. Equ. **32**, 266–291 (2016)